Check for updates

Jarl Beckers[1]
Thermo and Fluid Dynamics (FLOW) Faculty of Engineering,
Vrije Universiteit Brussel (VUB),
Pleinlaan 2, 1050 Brussels, Belgium;
Mobility Logistic and Automotive Technology Research Group (MOBI),
Department of Electrical Engineering and Energy Technology (ETEC),
Vrije Universiteit Brussel,
Pleinlaan 2, 1050 Brussels, Belgium
e-mail: jarl.beckers@vub.be

Bjorn Verrelst
Robotics & Multibody Mechanics Research Group (R & MM),
Faculty of Mechanical Engineering,
Vrije Universiteit Brussel,
Brussels 1050, Belgium
e-mail: bjorn.verrelst@vub.be

Francesco Contino
Institute of Mechanics, Materials and Civil Engineering (iMMC),
Université Catholique de Louvain (UCLouvain),
Place du Levant 2, 1348 Louvain-la-Neuve, Belgium
e-mail: francesco.contino@uclouvain.be

Joeri Van Mierlo
Mobility Logistic and Automotive Technology Research Group (MOBI),
Department of Electrical Engineering and Energy Technology (ETEC),
Vrije Universiteit Brussel,
Pleinlaan 2, 1050 Brussels, Belgium;
Flanders Make,
3001 Heverlee, Belgium
e-mail: joeri.van.mierlo@vub.be

Experimental Investigation of the Dynamics of a Slider-Crank Mechanism With Local Linear Force Input

Conventional implementation of slider-crank mechanisms result in high loads transmitted through the mechanical structure, inhibiting the design of compact and oil-free machines. Therefore, this research proposes to step away from the conventional, i.e., rotative, actuation and to investigate local linear actuation on the slider-component directly, while maintaining the kinematic link of the slider-crank configuration. In this work, the local linear actuating principle is evaluated experimentally where the goal is to obtain a continuous movement of the slider mechanism where Top Dead Center & Bottom Dead Center are reached and to minimize the loads transmitted through the mechanical structure. The non-isochronous transient behavior of a slider-crank mechanism loaded with a spring-damper element is detailed as well as the optimal working conditions at steady-state to achieve a reduced loading of the kinematic structure. By matching the operating frequency and resonance frequency of the system, a reduction of the loads transmitted through the system by 63% of the nominal spring load can be achieved. Further experimental (and multibody mechanical) investigation on the influence of flywheel exposes a clear trade-off between the sensitivity of the system and the transmission of the actuation force through the kinematic link. [DOI: 10.1115/1.4053146]

Keywords: slider-crank mechanism, flywheel, resonance, non-isochronous, linear actuation

1 Introduction

Slider-crank mechanisms have been investigated extensively in the past decades, due to their industrial applicability to convert rotary motion into linear motion or vice-versa in, e.g., gasoline engines and piston compressors [1]. However, in such applications, the mechanical structure is dimensioned to transmit and withstand the full power from piston to motor side and vice versa. As a result, fluid film bearings are often used to cope with the high loads transmitted through the system, complicating the possibility of a compact and hermetic solution [2,3]. Recent research proves furthermore the importance of dynamic analyses of such systems, with a focus on the relative motion in and minimization of loads acting on these joints. Varedi et al. performed dynamic investigations including the clearances in the joints to propose an optimization of the mass distribution of the links of a mechanism to reduce or eliminate the impact forces in the clearance joint [4]. Similarly, Zhao et al. propose a new numerical method for modeling and analysis of planar multibody system with lubricated revolute joints with the same goal of investigating the stability of the motion in the joints [5]. Yaqubi et al. investigated the possibility of using clearance control in joints accompanied with a second actuator on the connecting rod to reduce the vibrations and load on the first actuator [6]. Akbari et al. provide a more in depth analysis of the resonance of flexible connecting rod and proposes a piezo-actuator to suppress the vibrations [7]. Hong-Sen Ya proposes to step away from the traditional trajectories associated to a constant speed input by implementing a stepper motor. Properly designing the input speed of the mechanism, allows for the output motion to pass through a desired trajectory [8]. As a result, further research focuses on adequate actuation and (torque) control strategies to obtain a desired output profile [9,10]. Other possibilities have been investigated extensively such as the use of adjustable slider-crank mechanisms to obtain atypical trajectories [11–13]. Shao investigates such a configuration to actuate ankle exoskeletons through an inverted slider-crank mechanism [14]. Similarly, Sarigecili has demonstrated that by using a second (controlled) input force on the crank–connecting rod joint, a constant output force on the slider can be obtained, independent of the crank angle [15]. Soong goes a step further and details the design of flexible linkage mechanisms with a rotational input and a linear input combined [16] and similarly in Ref. [17] where such an innovative

[1]Corresponding author.

Contributed by the Applied Mechanics Division of ASME for publication in the Journal of Applied Mechanics. Manuscript received November 5, 2021; final manuscript received November 25, 2021; published online December 21, 2021. Assoc. Editor: Ahmet S. Yigit.

 Copyright © 2021 by ASME

Downloaded from asmedigitalcollection.asme.org/appliedmechanics/article-pdf/89/4/041002/6817042/jam_89_4_041002.pdf by University Catholique De Louvain-Uclouvain user on 04 November 2026

configuration is presented in a hybrid-driven mechanical press. Stepping away from the conventional use of a slider-crank mechanism provides thus the opportunity to match the output profile of the slider to the requirements of the system and to dimension the kinematic link accordingly [18]. This enables the search for the optimal design of the kinematic link to obtain a compact and lightweight structure for, e.g., gripper applications [19,20]. In a prior investigation to this paper [21], we went a step further and removed the rotational input completely. The research focused on the (multibody) dynamic analysis of local linear actuation on a slider-crank mechanism loaded with a spring-damper element. Actuating directly on the slider component, without rotational input, provides the opportunity to reduce the forces transmitted through the system. Instead of designing an optimal kinematic link for the application, the local linear actuation configuration allows to minimize the loads in the joints and reduce the power transmitted through the system significantly, compared to previous research [8,16,17,20]. This provides the possibility to downsize the mechanical structure and the entire machine in general. Furthermore, it would still allow to impose any desired trajectory (and associated control strategies), be it with mechanical limits. Maintaining this mechanical link provides a fail safe if an excessive force is imposed on the slider-component, which would allow to simplify control strategies compared to, e.g., free piston compressors [22], while guaranteeing that top and bottom dead center (TDC & BDC) are reached. The goal is to search for dynamic operating conditions, where the loads transmitted through the mechanical structure are minimized such that the kinematic link can be significantly downsized together with the new design guidelines associated with this innovative approach. As a result, we propose to validate the previously obtained [21] results experimentally, by adapting an existing practical set-up *RCK-1* [23] to further investigate the local linear actuation principle on a slider-crank mechanism loaded with a spring-damper element. The atypical implementation of the slider-crank mechanism calls for an investigation of the adapted working principle and associated possibilities. Therefore, the focus lies on the experimental characterization of the actuation principle and the consequences of such a configuration. By omitting the rotational input, a relationship between the operating frequency and the loads transmitted through the mechanical structure can be established for the different working regions. The non-isochronous transient oscillating behavior during a start-up is discussed at first in Sec. 2.1, followed by a detailed investigation of the optimal steady-state operating conditions in Sec. 2.2 where a significant reduction of the loads transmitted through the system has been achieved at resonance conditions. Particular attention will be paid to the transition of oscillating to rotating conditions as a sudden increase in operating frequency can be noticed. To conclude, the influence of the moment of actuation as well as the (polar inertia of the) flywheel on the loading of the system is highlighted in Sec. 3. A new design philosophy arises, where the trade-off between the sensitivity of the system and the loading of the kinematic link can be regulated with the polar inertia of the flywheel.

2 Experimental Set-Up

Previous research showed, by means of dynamic simulations, that by actuating locally on the slider component, the loads transmitted through the mechanical structure can be reduced by 90% at resonance while guaranteeing a continuous rotation of the crank rod [21]. However, further (experimental) investigation is required to fully comprehend the consequences of such a configuration and its associated dynamics. The conceptual layout is detailed in Fig. 1(*a*), where F_{act} represents the actuation force on the system. The idea is to utilize the dynamics of the system by launching the piston, by pushing and pulling it with a linear actuator, instead of controlling it rotationally, similarly to what occurs in combustion engines. The shape of the actuation current of the linear motor is illustrated in Fig. 1(*b*). The width of the actuation pulses is fixed throughout this paper, i.e., during 25% of the oscillation period a positive current (and thus force) is imposed and during 25% of the oscillation period a negative current is imposed (Fig. 1(*b*)). During the remaining 50%, no actuation force is acting on the system. This means that the frequency of actuation follows the oscillating (and eventually rotating) frequency of the system.

The experimental setup (Fig. 2) consists of a rotating shaft with a crank rod rigidly attached to the shaft (as well as a flywheel), a connecting rod connected to the crank rod and crosshead with two revolute joints and a crosshead which is supported by a translational joint to guide the linear movement. Two mechanical springs are attached to the system as external loads and a linear electromagnetic motor (designed in parallel research using the optimization algorithm detailed in Ref. [23]) is rigidly connected to provide the actuation forces to the system. A position sensor has been implemented which consists of three eddy current proximity probes radially placed on a 120 deg interval on a conical shaft with a decay of 1 mm. The combined measurement of the three radial probes is used to determine the axial position of the moving parts. A load cell (HBM U9C) has been incorporated to measure the loads transmitted through the mechanical structure, denoted as rod load. A *Performance Speedgoat Real Time Target Machine* has been used to control the *Inverter* with a switching frequency of 4 kHz to impose the desired currents to the linear motor. The sampling frequency of the *Speedgoat* is set to 10 kHz, both for the data-acquisition as for the control of the motor. In the post-processing of the results, a moving average filter has been implemented with a window of 50 samples to reduce the high frequency noise fluctuations on the signals.

The pre-tension of the springs has been set such that the system has its equilibrium position at half of the stroke, i.e., 22.1 mm. The specifications of the RCK-1 experimental set-up are detailed in Table 1.

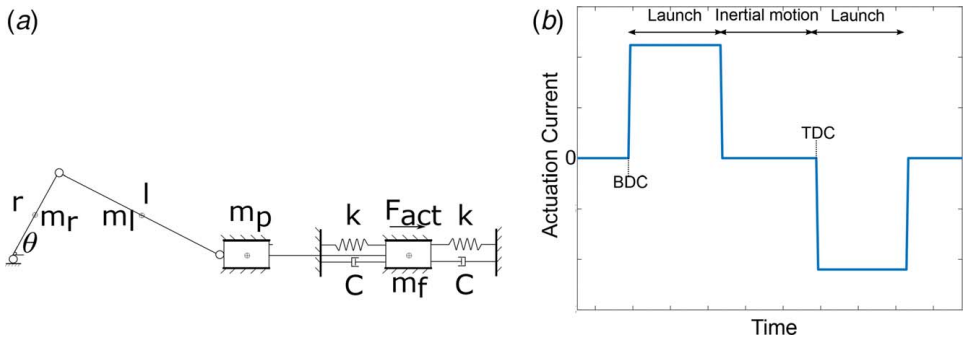


Fig. 1 Slider-crank mechanism with local linear actuation: (*a*) schematic drawing of the experimental set-up consisting of a slider-crank mechanism attached to two translational spring-damper elements and (*b*) concept of the bang-bang actuation current profile over 1 time period

Downloaded from asmedigitalcollection.asme.org/appliedmechanics/article-pdf/89/4/041002/6817042/jam_89_4_041002.pdf by University Catholique De Louvain-Uclouvain user on 04 November 2026

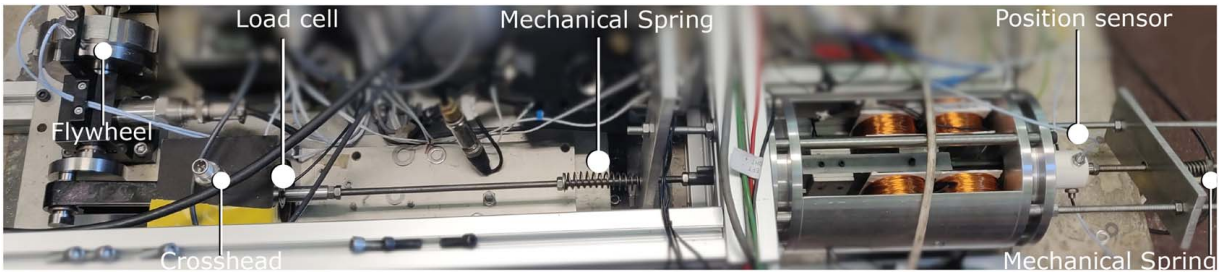


Fig. 2 Experimental layout of a slider-crank mechanism loaded with mechanical springs and rigidly connected to a linear actuator

To further detail the operating principle and test campaign, an example of an experimental start-up procedure to steady-state is illustrated in Figs. 3 and 4 and discussed below.

The numbering below corresponds to the numbers indicated in Figs. 3 and 4.

(1) The initial position of the rotor is close to TDC due to the fact that the linear motor provides a static force at 0 A pulling the entire system toward the top singular position (analogous to a cogging torque in permanent magnet motors). To focus the investigation on the non-linear dynamics of the slider-crank mechanism loaded with mechanical springs, a counteracting current control strategy has been implemented to compensate this electromagnetic spring (force) associated with the linear motor. Activating this compensation at around 5 s, results in a sudden movement of the rotor position to half the stroke, i.e., the resting position of the mechanical system due to the two spring forces acting on the system.
(2) A pulse-shaped reference current (Fig. 1(*b*)) is then superposed on the compensating current to provide the desired actuation force on the system. The amplitude of the current pulse is systematically increased, gradually increasing the oscillation amplitude of the system. The envelope curve of the imposed actuation current is illustrated in Fig. 4.
(3) At around 45 s, the oscillation amplitude reaches the full stroke of the system, i.e. 44.2 mm, and the crank rod starts rotating.
(4) Afterwards, the current is decreased to adapt the operating frequency of and loads transmitted through the system (Fig. 4).
(5) To conclude, when the imposed current is smaller than the minimal one required to maintain the rotation, the crank rod starts oscillating again.

During the transient, the loads systematically increase accordingly with the oscillation amplitude. Once rotating conditions are achieved, there exists an optimal actuation current to significantly decrease the loads transmitted through the system, this zone has been indicated with a transparent gray box in Fig. 4. The following sections will provide a more in depth investigation by focusing on the frequency analysis of the non-isochronous oscillating movement (transient) as well as on the optimal operating frequency during rotating conditions (steady-state), which yields a reduced loading of the kinematic link.

2.1 Transient Analysis. During start-up, the oscillation amplitude is gradually increased by inserting more and more energy in the system until rotation of the crank rod is achieved. However, during the oscillating transient, similarly to a pendulum, the oscillation frequency decreases with increasing oscillation amplitude. This phenomenon is shown in Fig. 5, where the frequency evolution of the experiment detailed in the previous section is plotted as a function of time.

During nominal working conditions (i.e., continuous rotation of the crank rod), the crank rod and flywheel will barely accelerate and decelerate and the eigenfrequency of the system can then be approximated by Eq. (1), assuming the oscillations of the connecting rod are small:

$$f_{eigen,approximated} = \frac{1}{2\pi}\sqrt{\frac{2k_{spring}}{m_f + m_p + m_l}} = 8 \text{ Hz} \tag{1}$$

However, during transient, the crank rod and flywheel participate to the oscillating movement and as a result the corresponding oscillating frequency will be much lower than the rotating frequency of the system. This non-isochronous oscillating behavior has been detailed in preceding research [21] and is derived in Appendix A. The oscillation period T_{os} of a slider-crank mechanism loaded with a mechanical spring can be described as a function of the starting angle θ_0 and the mechanical parameters of its components, i.e., masses and moments of inertia of the different parts and the stiffness of the springs. The potential energy stored in the crank and connecting rod and in the mechanical springs at θ_0 is converted into kinetic energy of the moving parts. By assuming a lossless system, this oscillating movement can be completely quantified with the conservation of energy equation yielding Eq. (2).

$$T_{os} = \int_{\theta_{os}} \sqrt{\frac{\frac{1}{2}\left(I_r + I_{fly} + I_l\frac{r^2\cos^2\theta}{a^2} + m_p\left(-r\sin\theta - \frac{r^2\sin\theta\cos\theta}{a}\right)^2 + m_l\left(\left(r\sin\theta + \frac{\frac{1}{2}r^2\sin\theta\cos\theta}{a}\right)^2 + \left(\frac{r}{2}\cos\theta\right)^2\right)\right)}{((m_r + m_l)g\frac{r}{2}\sin\theta_0 + \frac{k}{2}(r\cos\theta_0 + a_0 - l)^2 - (m_r + m_l)g\frac{r}{2}\sin\theta - \frac{k}{2}(r\cos\theta + a - l)^2)}}\, d\theta \tag{2}$$

with

$$a = \sqrt{l^2 - r^2\sin^2\theta} \tag{3}$$

Solving Eq. (2) numerically for the values indicated in Table 1 allows to determine the theoretical oscillation frequency as a function of the starting angle θ_0. Figure 6 shows indeed that a larger oscillation amplitude results in a lower oscillation frequency.

Downloaded from asmedigitalcollection.asme.org/appliedmechanics/article-pdf/89/4/041002/6817042/jam_89_4_041002.pdf by University Catholique De Louvain-Ucl Louvain user on 04 November 2026

Table 1 Specifications of the slider-crank mechanism analysis

Length crank rod r (mm)	22.1
Length connecting rod l (mm)	127.0
Mechanical stiffness spring k (N/mm)	3.19
Maximum static spring force $F_{s,max}$ (N)	141
Mass crank rod m_r (kg)	0.06
Mass connecting rod m_l (kg)	0.30
Mass crosshead m_p (kg)	0.72
Mass flotor and permanent magnets m_f (kg)	1.50
Mass flywheel m_{fly} (kg)	2.10
Polar inertia flywheel I_{fly} (kg mm^2)	5000
Polar inertia crank rod I_r (kg mm^2)	13
Polar inertia connecting rod I_l (kg mm^2)	403

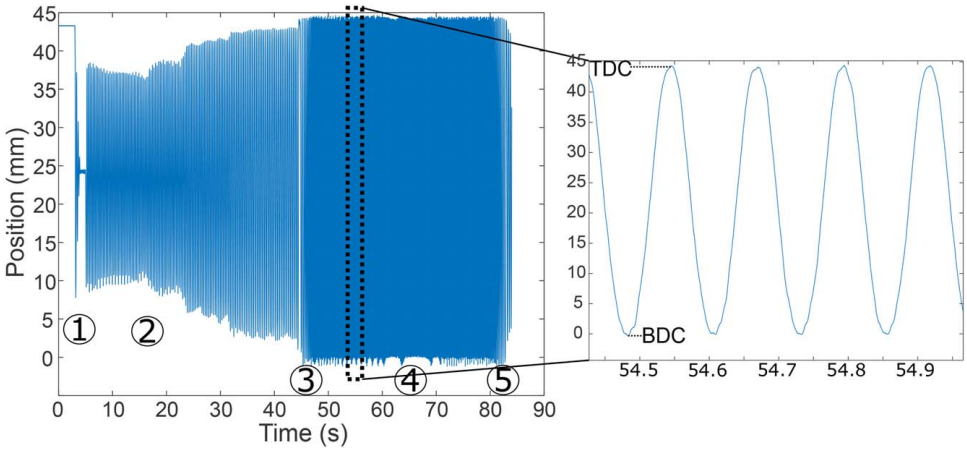


Fig. 3 Position evolution over time where the current and thus actuation force has been systematically increased to achieve rotation of the crank rod

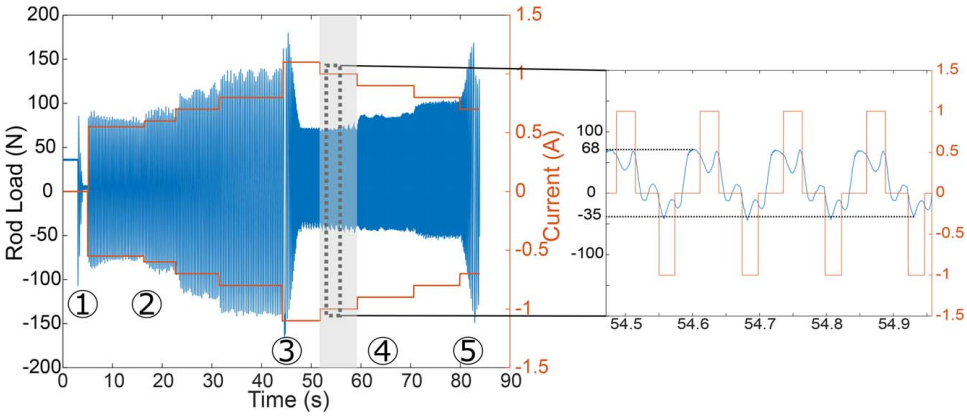


Fig. 4 Rod load evolution over time together with the envelop curve of the imposed actuation current. The zoom on the right represents the actual imposed current in agreement with Fig. 1(*b*).

This contribution of the flywheel and crank rod can also be explained in a more pragmatic manner. In torsion vibration analyses of combustion engines, an equivalent polar moment of inertia of the piston can be computed using the conservation of energy formulation. An identical approach can be used here to compute an equivalent linear mass M_{eq} from the polar inertia I_p of the flywheel and crank rod respectively to investigate the linear vibration behavior of the system:

$$M_{eq} = \frac{2I_p}{r^2} \tag{4}$$

Using Eq. (4) to calculate the equivalent mass of the flywheel (the equivalent mass of the crank rod is negligible compared to the flywheel) using the polar inertia detailed in Table 1 and incorporating this mass in Eq. (1), yields an approximated eigenfrequency during the transient of

$$f_{eigen,approximated} = \frac{1}{2\pi}\sqrt{\frac{2k_{spring}}{m_f + m_p + m_l + M_{eq,fly}}} = 2.7\,\text{Hz} \tag{5}$$

Of course, Eq. (4) provides an averaged value of the equivalent mass of the flywheel and does not take into account the non-isochronous movement of the system highlighted in Figs. 5 and 6. Nevertheless, together with Eq. (2), it contributes to the

Downloaded from asmedigitalcollection.asme.org/appliedmechanics/article-pdf/89/4/041002/6817042/jam_89_4_041002.pdf by University Catholique De Louvain-Ucl louvain user on 04 November 2026

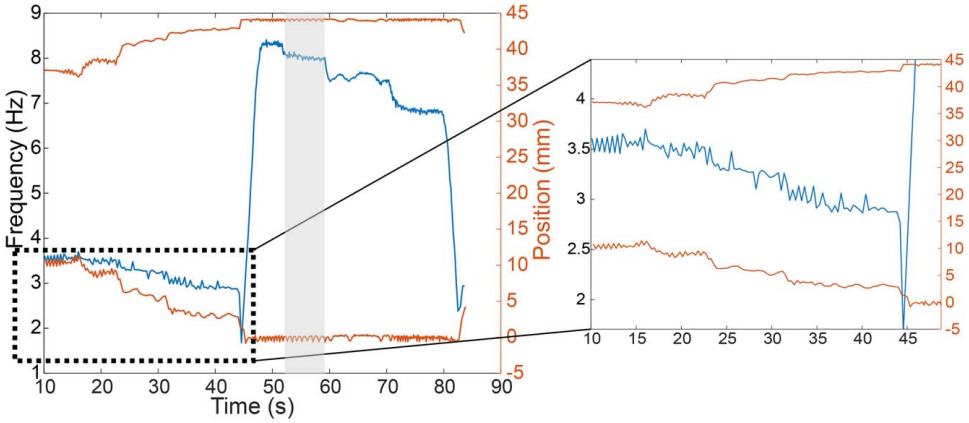


Fig. 5 The evolution of the operating frequency over time during a start-up procedure together with the envelope curve of the corresponding oscillation amplitude

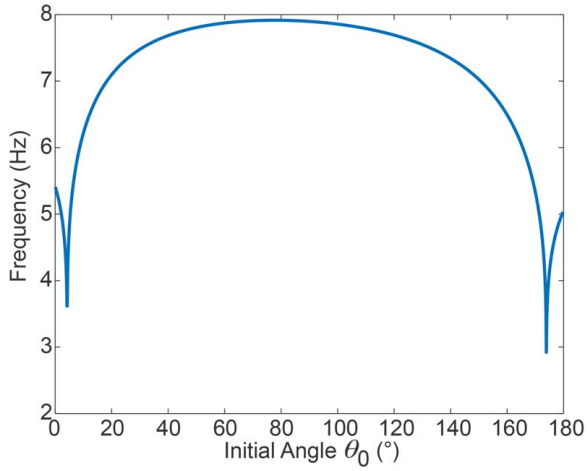


Fig. 6 Oscillating frequency as a function of the release angle θ_0

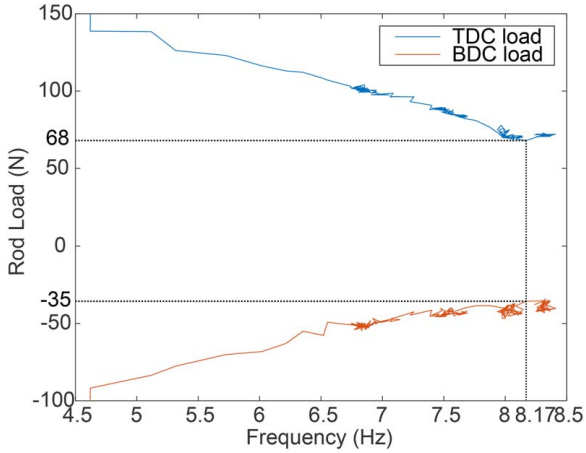


Fig. 7 Rod load as a function of the operating frequency during steady-state conditions

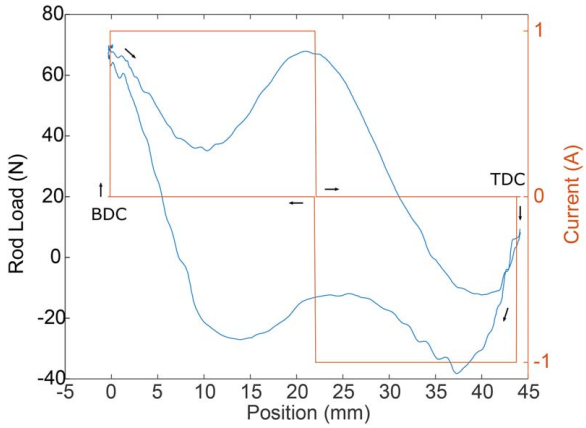


Fig. 8 Rod load as a function of the position for the zoom in Figs. 3 and 4

understanding of the sudden frequency shift at the moment the crank rod stops oscillating and starts rotating (i.e., at ≈45 s in Fig. 5). During the entire transient, the flywheel dominates the oscillating movement as well as the natural frequency of the system. However, from the moment the crank rod, and flywheel accordingly, starts rotating, it no longer performs an oscillating movement. As a result, the oscillating mass instantaneously reduces significantly and the natural frequency of the system jumps to the one approximated in Eq. (1). This phenomenon can also clearly be observed in the video of the experiment at around 45 s.[2]

2.2 Steady-State Analysis. During steady-state rotative conditions, an optimal actuation current exists to minimize the loads in the system. More precisely, the closer the operating frequency of the system to the natural frequency, the lower the rod load will be [21]. This optimal zone has been indicated by a gray box in Figs. 4 and 5. Decreasing the actuation current from 1.2 A to 1.1 A, i.e., entering this optimal zone, results in a (small) decrease in rod load as we approach the resonance frequency of the system. The nominal load of the system is highlighted in Table 1 where the maximum spring force is approximately [–140 +140] N. The resulting rod load however, at 8.17 Hz operating frequency and an actuation current of [–1.1 1.1] A, is reduced to [–35 68] N. A clear reduction of 63%. Nevertheless, due to the fact that, in order to guarantee rotation, a certain acceleration is required at TDC and BDC to avoid getting stuck in a singular configuration, a full reduction of the rod load will not be possible. Furthermore, the load cell is placed between the crosshead and rotor of the linear motor (Fig. 2). As a result, a part of the internal inertia forces (those of the crosshead) is measured in the load cell while not being transmitted to the joints, if the resonance conditions are met. Exiting this gray zone by further decreasing the actuation current, i.e., decreasing the operating frequency (Fig. 5), results in

[2]https://www.youtube.com/watch?v=lr4LixquMHQ

Downloaded from asmedigitalcollection.asme.org/appliedmechanics/article-pdf/89/4/041002/6817042/jam_89_4_041002.pdf by University Catholique De Louvain-Uclouvain user on 04 November 2026

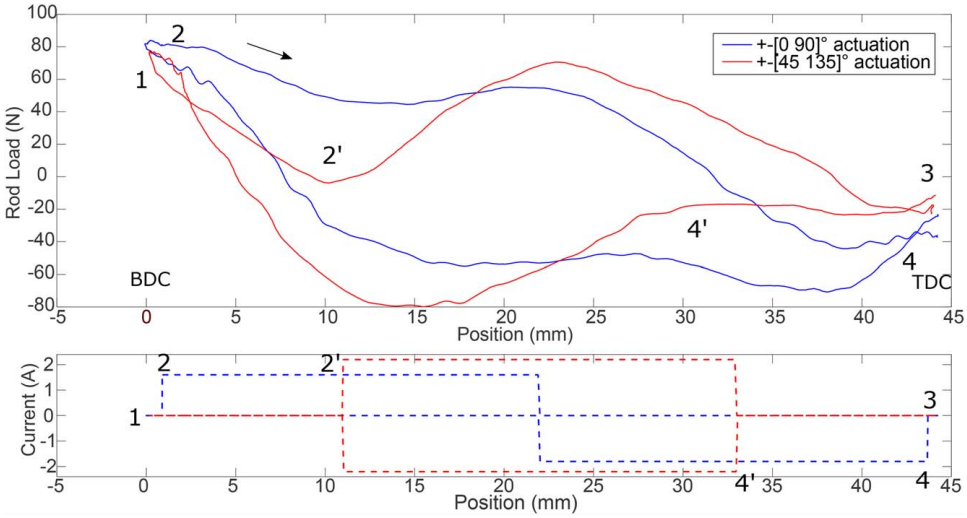


Fig. 9 Comparison of rod load profiles as a function of the position, where the actuation moment is varied from [0 90] deg to [45 135] deg

a clear increase of the rod load visible at ≈60 s and 70 s. Excessively increasing the actuation current would have a similar result as the operating frequency would again deviate from the natural frequency as it goes up, resulting again in an increase of the transmitted rod load. The rod load versus frequency (during steady-state rotating conditions) plot of the experimental configuration detailed above is highlighted in Fig. 7.

3 Discussion

The rod load profile visible in Fig. 4 requires a more in depth investigation and associated discussion. Plotting the rod load profile as function of the position in Fig. 8 shows that the maximum positive rod load is at BDC where the kinematic structure limits any further movement and thus a reaction force to inverse the movement causes the ≈70 N rod load. However, the maximum negative rod load is only after TDC is passed, when the negative actuation current/force is imposed. Due to the presence of a flywheel, the system is reluctant to changes once it is rotating smoothly. In other words, the actuation force will be partially transmitted through the mechanical structure and will thus be visible in the measured rod load profile. Furthermore, this transmission will depend on the position of actuation, or more precisely on the configuration of the slider-crank mechanism. Until now the actuation current (and thus force) has been applied from TDC to 90 deg crank angle and from BDC to −90 deg. Therefore, the two following experimental investigations are detailed in the following sections:

(1) The influence of the actuation position on the rod load profile.
(2) The influence of the flywheel on the rod load profile.

3.1 Actuation Force Position. To investigate the influence of the actuation position on the transmission of the actuation force in the kinematic link, a comparison between two experiments has been detailed below. The main difference between the two experiments is the moment of actuation. In the first experiment, the actuation takes place from TDC to 90 deg crank angle and from BDC to −90 deg. In the second experiment, the actuation takes place from 45 deg to 135 deg crank angle and from −45 deg to −135 deg. The results illustrated in Fig. 9 do not correspond to ideal operating conditions, i.e., minimal rod load.

A first important comment is the amplitude of the actuation current is different between the two experiments. This is a consequence of the non-linear force profiles of the motor with respect to the the current and position of the rotor. Therefore the comparison is made between the two experiments where the operating frequency is the same, i.e., 7.2 Hz. As a result, a higher current is needed from 45 deg to 135 deg to obtain the same operating frequency. The fact that the operating frequency is the same, the same rod load can be observed at TDC and BDC in the two curves. Let us detail the [0 90] deg-profile first. The numbering below corresponds to the numbers indicated in Fig. 9.

(1) The piston is at BDC position and the rod load is maximal due to the acceleration still present in the singular configuration associated with the frequency mismatch with respect to the resonance frequency.
(2) A positive actuation current is imposed to launch the piston towards TDC where the rod load decreases a little bit at first but remains on a plateau due to the actuation force still acting on the system and which is transmitted through the mechanical structure. After 22 mm, the rod load decreases as the actuation current is 0 until TDC is reached.
(3) The piston is at TDC position and the rod load is minimal, where the reasoning is identical to 1.
(4) A negative actuation current is imposed until 22 mm, inhibiting the rod load to decrease further until actuation is stopped.

An identical reasoning can be made on the [45, 135] deg profile. At around 11 mm, the positive actuation takes place (2′) resulting in an increase of the rod load. Similarly at 4′ where the negative actuation force is imposed, results in a decrease of the rod load. This visibility of the actuation force in the rod load profile becomes particularly interesting when taking into account the influence of the flywheel of the system, detailed in the following section. As an extension of the experimental results, for the sake of clearness, the phenomenon is also investigated using a multibody model of the slider-crank mechanism loaded with a spring-damper element (discussed in detail in Ref. [21]). This allows to qualitatively

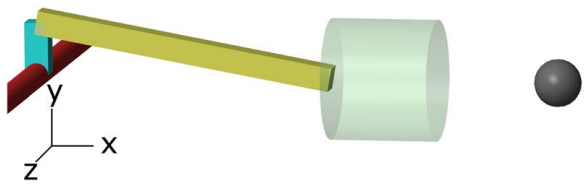


Fig. 10 Simscape lay-out of a slider-crank mechanism loaded with a mechanical spring-damper element [21]

Downloaded from asmedigitalcollection.asme.org/appliedmechanics/article-pdf/89/4/041002/6817042/jam_89_4_041002.pdf by University Catholique De Louvain-Uclouvain user on 04 November 2026

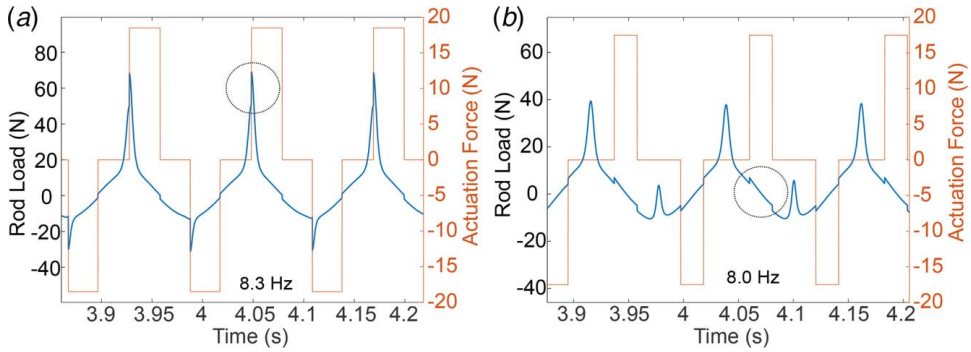


Fig. 11 Multibody simulated rod load profiles in *Simscape* to highlight the transmission of the actuation force in the mechanical structure: (*a*) steady-state simulated rod load profile for a [0 90] deg actuation and (*b*) steady-state simulated rod load profile for a [45 135] deg actuation

clarify the obtained experimental results. The model is illustrated in Fig. 10 and consists of a shaft connected to the ground with a revolute joint, a crank rod rigidly connected to the shaft, a connecting rod connected to the crank rod and piston with two revolute joints and a piston whose motion is limited using a translational joint with respect to the ground. The spring-damper element has been implemented as a linear force acting between the piston and ground, visualized by the "dummy" gray ball. The system has its resting position at half of the stroke [21]. However, no clearances are incorporated in the joints, i.e., rigid joints, contrarily to Refs. [4,5], which would give a more accurate representation of the impact forces in the joints. Nevertheless, a detailed analysis on the modeling of the joints is outside the scope of this research. The implemented numerical configuration is listed in Table 1, where the polar inertia of the flywheel is added to the polar inertia of the crank rod and similarly the mass of the flotor m_f is added to the mass of the crosshead/piston m_p.

The simulated rod load is plotted as a function of time for a [0 90] deg actuation and [45 135] deg actuation in Figs. 11(*a*) and 11(*b*), respectively. The point of interest has been encircled in both

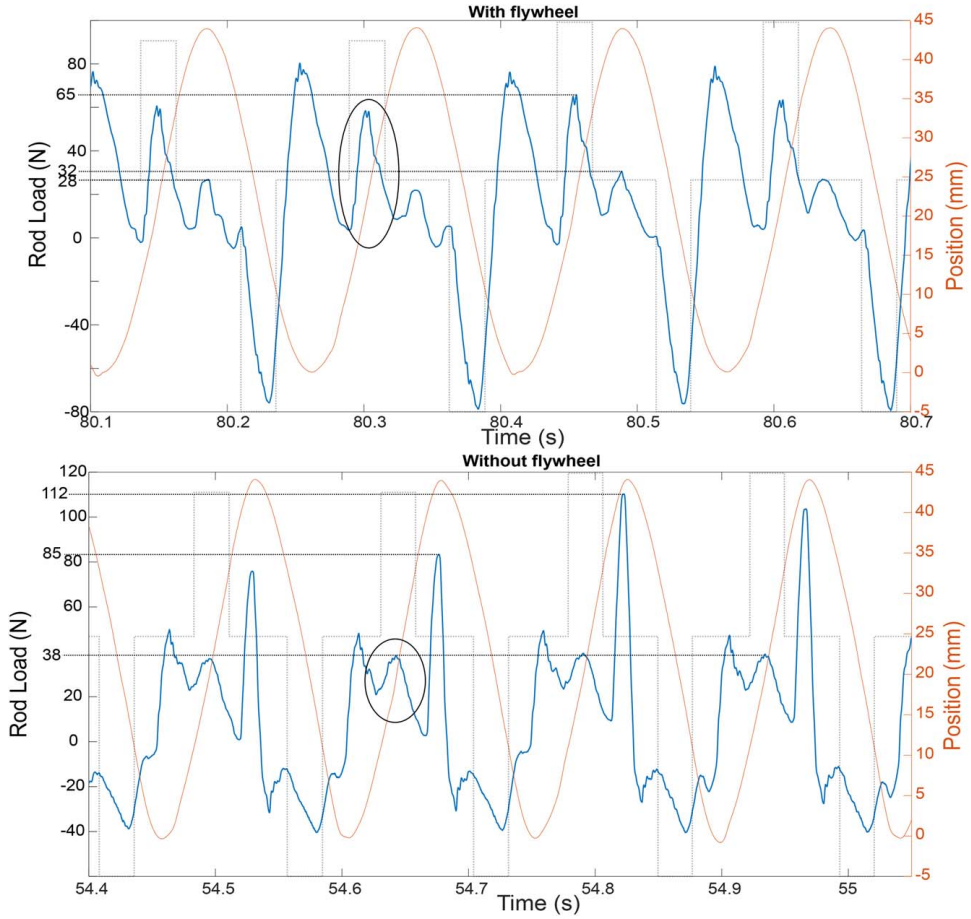


Fig. 12 Comparison between the experimentally obtained rod load profiles of the flywheel and no-flywheel-case, respectively, to highlight the sensitivity of the system and the transmission of the actuation force. The actuation current and position have been added for the sake of clearness.

Downloaded from asmedigitalcollection.asme.org/appliedmechanics/article-pdf/89/4/041002/6817042/jam_89_4_041002.pdf by University Catholique De Louvain-Ucl louvain user on 04 November 2026

graphs to highlight the discontinuity in the rod load associated with the transmission of the actuation force. This jump in rod load is more sudden compared to the experimental results due to the fact that a square wave actuation force profile has been imposed instead of a square wave actuation current. Figures 11(*a*) and 11(*b*) prove that the actuation force is much more visible in the rod load profile when actuating close to the singular configurations. The [45 135] deg actuation strategy provides furthermore the opportunity to significantly downsize the linear motor. Since no forces are required between 0 deg and 45 deg and analogously between 135 deg and 180 deg, the actuator can be designed on approximately 50% of the stroke, compared to a full stroke position controlled application.

3.2 Flywheel Influence. To conclude this research, a final elaboration of the previous results is detailed as well as the influence of the flywheel on the rod load profile in general. The following comparison consists of two experiments where the actuation current amplitude has been increased in a step of 0.2 A to evaluate the sensitivity of the system. The actuation takes place in both cases between 45 deg and 135 deg crank angle. The difference between the two cases is that in the second case the flywheel, indicated in Table 1 and Fig. 2, has been removed. Figure 12 depicts two rod load cycles before and two rod load cycles after the amplitude of the current pulse has been increased. For the sake of clearness, the current pulses have been incorporated in Fig. 12, without any values, to highlight the moment of amplitude change.

The upper graph of Fig. 12 shows that an increase of current of 0.2 A results in an marginal increase of rod load at TDC of ≈4 N (from 28 N to 32 N) compared to an increase of ≈ 27 N (from 85 N to 112 N) in the no-flywheel-case indicated in the lower graph. However, for an identical actuation force, since the actuation current is identical as well as the moment of actuation between the two experiments, this force is much more visible in the rod load, i.e., 65 N, in the flywheel-case compared to 38 N in the no-flywheel-case. These last absolute values might however give a false representation as they are a combination of the rod load as a consequence of the spring and inertia forces of the system and of the rod load due to the transmission of the actuation force. Nevertheless, upon evaluating the increase of the rod load upon actuation, indicated by the circles, the flywheel-case shows a much larger and steeper increase at the moment of actuation compared to the no-flywheel-case. In other words, the flywheel is reluctant to changes when applying an actuation force and results thus in a reaction force in the mechanical structure proportional to the polar inertia of the flywheel. However, it also relaxes the system since a small change (e.g., possible error in a controller) results in a marginal increase of the rod load of the system. As a result, a trade-off pops up between the transmission of the actuation force in the kinematic link and the sensitivity of the system. Again, for the sake of clearness, a set of multibody simulations have been performed for the flywheel and no-flywheel-case to further detail the sensitivity of the system. The actuation force has been gradually increased to adapt the operating frequency and the rod load at TDC and BDC has been determined accordingly. The results detailed in Fig. 13 prove indeed that a larger flywheel (or polar inertia in general) decreases the sensitivity of the system as the rod load stays within acceptable limits for a wider frequency range and thus actuation amplitude range. Figure 13 only contains points where steady-state rotation has been achieved. In other words, without flywheel, no operation under ≈7 Hz is possible since there is not enough inertia to go through the singular configurations of the system.

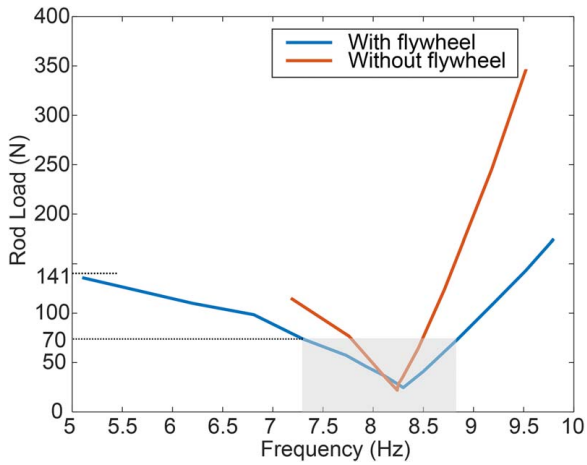


Fig. 13 Simulated rod load as a function of the operating frequency for the flywheel and no-flywheel-case

These results enable a new design strategy with respect to a traditional use of slider-crank mechanisms and associated flywheels. This trade-off between sensitivity and loading of the kinematic link, provides the opportunity to make the system more flexible to changing requirements of the customer, e.g., flow requirements of a piston compressor. More specifically, a certain upper limit for the rod load can be defined per design, e.g., 50% of the nominal spring force as indicated in Fig. 13, providing an operating region around the resonance frequency (indicated by the gray zone). When minor changes of the operating frequency are required during operation, i.e., deviating from the minimal loading conditions, the increase in rod load can be tolerated under the preset limit. This allows to dimension the mechanical structure for the preset maximum rod load as well as the flywheel for the desired sensitivity of the system.

4 Conclusion

This paper proposed to step away from the traditional use of a slider-crank mechanism by experimentally investigating the influence of a local linear actuation on the slider, loaded with a mechanical spring. In a first step, a general experiment has been discussed to detail the non-isochronous movement during transient due to the increasing oscillation amplitude as well as the sudden frequency increase upon rotation due to the absence of contribution of the flywheel to the linear vibration. During steady-state conditions, an operating frequency was found, close to the resonance frequency of the system, in which the loads transmitted through the mechanical structure could be reduced by 63%. Afterward a more in depth (multibody and experimental) investigation of the rod load profile has been discussed with a focus on the instant of actuation. To conclude, the flywheel has been removed to study the effect of the polar inertia on the system. A clear trade-off between the sensitivity of the system and the visibility of actuation force in the rod load was found.

Acknowledgment

Flanders Innovation & Entrepreneurship Agency (VLAIO) is gratefully acknowledged for its support within the Baekeland-mandate **HBC.2018.2055**. Furthermore, we acknowledge *Flanders Make* for the support of our team.

Conflict of Interest

There are no conflicts of interest.

Data Availability Statement

The authors attest that all data for this study are included in the paper. The authors attest that all data for this study are included in the paper.

Downloaded from asmedigitalcollection.asme.org/appliedmechanics/article-pdf/89/4/041002/6817042/jam_89_4_041002.pdf by University Catholique De Louvain-Uclouvain user on 04 November 2026

Nomenclature

f = frequency [Hz]
k = spring stiffness [N/m]
l = length connecting rod [m]
m = mass [kg]
r = length crank rod [m]
v = velocity [m/s]
x = position [m]
C = damping coefficient [Ns/m]
F = force [N]
I = moment of inertia [kg m^2]
T = period [s]
θ = Crank angle, deg
ϕ = Connecting rod angle, deg

Subscripts

act = actuation
eq = equivalent
f = flotor
fly = flywheel
l = connecting rod
max = maximum
os = oscillation
p = piston
r = crank
s = static
spring = spring

Appendix A: Derivation Oscillation Period of a Slider-Crank Mechanism Loaded With a Mechanical Spring [21]

Starting from the kinetic and potential energy of the slider-crank system displayed in Fig. 14:

$$\begin{aligned} T &= \tfrac{1}{2} I_r \dot{\theta}^2 + \tfrac{1}{2} I_l \dot{\phi}^2 + \tfrac{1}{2} m_p v_p^2 + \tfrac{1}{2} m_l v_l^2 \\ V &= m_r g \tfrac{r}{2} \sin(\theta) + m_l g \tfrac{l}{2} \sin(\phi) + \tfrac{k}{2} \Delta x_p^2 \end{aligned} \tag{A1}$$

with

- $v_l = \sqrt{\left(r \sin\theta + \dfrac{r^2 \sin\theta \cos\theta}{2\sqrt{l^2 - r^2 \sin^2\theta}} \right)^2 + \left(\tfrac{r}{2}\cos\theta\right)^2}\,\dot{\theta}$
- $\dot{\phi} = \dfrac{r\cos\theta}{l\sqrt{1 - \left(\dfrac{r}{l}\sin\theta\right)^2}}\,\dot{\theta}$
- $v_p = \left(-r\sin\theta - \dfrac{r^2 \sin\theta\cos\theta}{\sqrt{l^2 - r^2\sin^2\theta}} \right)\dot{\theta}$
- $\Delta x_p = r\cos\theta + \sqrt{l^2 - r^2\sin^2\theta} - l$

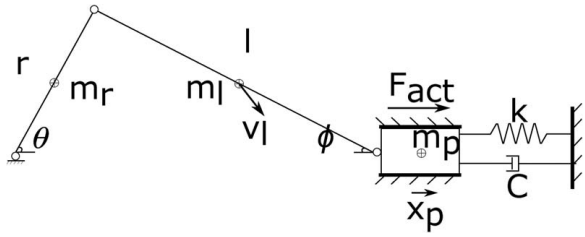


Fig. 14 Schematic drawing of a slider-crank mechanism attached to a translational spring-damper element [21]

Substituting the equalities above in the potential and kinetic energy formulations together with $l\sin\phi = r\sin\theta$ and denoting the recurring term $\sqrt{l^2 - r^2\ \sin(\theta)^2}$ as a, the following equations are obtained:

$$\begin{aligned} a &= \sqrt{l^2 - r^2\ \sin\theta^2} \\ \frac{da}{d\theta} &= -\frac{r^2 \sin\theta\cos\theta}{a} \end{aligned} \tag{A2}$$

$$T = \frac{1}{2} I_r \dot{\theta}^2 + \frac{1}{2} I_l \frac{r^2\cos^2\theta}{a^2}\dot{\theta}^2 + \frac{1}{2} m_p \left(-r\sin\theta - \frac{r^2\sin\theta\cos\theta}{a} \right)^2 \dot{\theta}^2 + \frac{1}{2}\left(\left(r\sin\theta + \frac{\frac{1}{2}r^2\sin\theta\cos\theta}{a} \right)^2 + \left(\frac{r}{2}\cos\theta\right)^2 \right)\dot{\theta}^2$$

$$V = m_r \frac{r}{2} g\sin\theta + m_l \frac{r}{2} g\sin\theta + \frac{k}{2}(r\cos\theta + a - l)^2 \tag{A3}$$

Using the conservation of energy theorem, with $a_0 = \sqrt{l^2 - r^2\sin^2\theta_0}$:

$$\begin{aligned} &\frac{1}{2} I_r\ \dot{\theta}^2 + \frac{1}{2} I_l \frac{r^2\cos^2\theta}{a^2}\dot{\theta}^2 + \frac{1}{2} m_p \left(-r\sin\theta - \frac{r^2\sin\theta\cos\theta}{a} \right)^2 \dot{\theta}^2 \\ &+ \frac{1}{2} m_l \left(\left(r\sin\theta + \frac{\frac{1}{2}r^2\sin\theta\cos\theta}{a} \right)^2 + \left(\frac{r}{2}\cos\theta\right)^2 \right)\dot{\theta}^2 \\ &= (m_r + m_l) g \frac{r}{2}\sin\theta_0 + \frac{k}{2}\ (r\cos\theta_0 + a_0 - l)^2 \\ &- (m_r + m_l) g \frac{r}{2}\sin\theta - \frac{k}{2}\ (r\cos\theta + a - l)^2 \end{aligned} \tag{A4}$$

Isolating $\dot{\theta}$ and integrating over one cycle θ_{cycle} yields the oscillation period T_{os} as function of the starting angle θ_0:

$$T_{os} = \int_{\theta_{cycle}} \sqrt{\frac{\frac{1}{2}\left(I_r + I_l \frac{r^2\cos^2\theta}{a^2} + m_p \left(-r\sin\theta - \frac{r^2\sin\theta\cos\theta}{a} \right)^2 + m_l \left(\left(r\sin\theta + \frac{\frac{1}{2}r^2\sin\theta\cos\theta}{a} \right)^2 + \left(\frac{r}{2}\cos\theta\right)^2 \right) \right)}{(m_r + m_l) g \frac{r}{2}\sin\theta_0 + \frac{k}{2}(r\cos\theta_0 + a_0 - l)^2 - (m_r + m_l) g \frac{r}{2}\sin\theta - \frac{k}{2}(r\cos\theta + a - l)^2)}}\, d\theta \tag{A5}$$

Downloaded from asmedigitalcollection.asme.org/appliedmechanics/article-pdf/89/4/041002/6817042/jam_89_4_041002.pdf by University Catholique De Louvain-Uclouvain user on 04 November 2026

References

[1] Hartenberg, R., and Danavit, J., 1964, *Kinematic Synthesis of Linkages*, New York, McGraw-Hill.

[2] Liang, K., Stone, R., Hancock, W., Dadd, M., and Bailey, P., 2014, "Comparison Between a Crank-Drive Reciprocating Compressor and a Novel Oil-Free Linear Compressor," Int. J. Refrig., **45**(1), pp. 25–34.

[3] Bailey, P., Dadd, M., and Stone, C., 2009, "An Oil-Free Linear Compressor for Use With Compact Heat Exchangers," International Conference on Compressors and Their Systems, pp. 259–268.

[4] Varedi, S., Daniali, H., Dardel, M., and Fathi, A., 2015, "Optimal Dynamic Design of a Planar Slider-Crank Mechanism With a Joint Clearance," Mech. Mach. Theory., **86**(1), pp. 191–200.

[5] Zhao, B., Zhou, K., and Xie, Y.-B., 2016, "A New Numerical Method for Planar Multibody System With Mixed Lubricated Revolute Joint," Int. J. Mech. Sci., **113**(1), pp. 105–119.

[6] Yaqubi, S., Dardel, M., and Daniali, H. M., 2016, "Nonlinear Dynamics and Control of Crank–Slider Mechanism With Link Flexibility and Joint Clearance," Proc. Inst. Mech. Eng., Part C: J. Mech. Eng. Sci., **230**(5), pp. 737–755.

[7] Akbari, S., Fallahi, F., and Pirbodaghi, T., 2016, "Dynamic Analysis and Controller Design for a Slider–Crank Mechanism With Piezoelectric Actuators," J. Comput. Design Eng., **3**(4), pp. 312–321.

[8] Yan, H.-S., and Chen, W.-R., 2000, "On the Output Motion Characteristics of Variable Input Speed Servo-Controlled Slider-Crank Mechanisms," Mech. Mach. Theory., **35**(4), pp. 541–561.

[9] Wang, X., Ma, Q., and Zhu, Z., 2007, "Low Noise Control of Servo Press," IECON 2007—33rd Annual Conference of the IEEE Industrial Electronics Society, pp. 833–838.

[10] Ha, J.-L., Fung, R.-F., Chen, K.-Y., and Hsien, S.-C., 2006, "Dynamic Modeling and Identification of a Slider-Crank Mechanism," J. Sound. Vib., **289**(4), pp. 1019–1044.

[11] Shoup, T. E., 1984, "The Design of An Adjustable, Three Dimensional Slider Crank Mechanism," Mech. Mach. Theory., **19**(1), pp. 107–111.

[12] Kay, F. J., and Haws, R. E., 1975, "Adjustable Mechanisms for Exact Path Generation," J. Eng. Ind., **97**(2), pp. 702–707.

[13] Zhou, H., and Ting, K.-L., 2002, "Adjustable Slider-Crank Linkages for Multiple Path Generation," Mech. Mach. Theory., **37**(5), pp. 499–509.

[14] Shao, Y., Zhang, W., Su, Y., and Ding, X., 2021, "Design and Optimisation of Load-Adaptive Actuator With Variable Stiffness for Compact Ankle Exoskeleton," Mech. Mach. Theory, **161**(1), p. 104323.

[15] Sarigecili, M. I., and Akcali, I. D., 2019, "Development of Constant Output-Input Force Ratio in Slider–Crank Mechanisms," Inverse Prob. Sci. Eng., **27**(5), pp. 565–588.

[16] Soong, R.-C., 2012, "A Design Approach for Flexible Linkage Mechanisms With a Rotational and a Linear Input," Adv. Sci. Lett., **9**(1), pp. 499–504.

[17] Soong, R.-C., 2014, "The New Hybrid-Driven Mechanical Presses," J. Vibroeng., **16**(2), pp. 945–953.

[18] Arakelian, V., and Zhang, Y., 2019, "An Improved Design of Gravity Compensators Based on the Inverted Slider-Crank Mechanism," ASME J. Mech. Rob., **11**(3), p. 034501.

[19] Bai, L., Wan, H., Chen, X., Zheng, J., Xin, L., Deng, Y., and Sun, Y., 2021, "Design and Experiment of a Deformable Bird-Inspired UAV Perching Mechanism," J. Bionic Eng., **59**(1), pp. 1–13.

[20] Chi, W., Low, K. H., Hoon, K. H., and Tang, J., 2014, "An Optimized Perching Mechanism for Autonomous Perching With a Quadrotor," IEEE International Conference on Robotics and Automation (ICRA), pp. 3109–3115.

[21] Beckers, J., Verstraten, T., Verrelst, B., Contino, F., and Van Mierlo, J., 2021, "Analysis of the Dynamics of a Slider-Crank Mechanism Locally Actuated With An Act-and-Wait Controller," Mech. Mach. Theory, **159**(1), p. 104253.

[22] Liang, K., 2017, "A Review of Linear Compressors for Refrigeration," Int. J. Refrige.-Revue Int. Du Froid, **84**(1), pp. 253–273.

[23] Beckers, J., Coppitters, D., De Paepe, W., Contino, F., Van Mierlo, J., and Verrelst, B., 2020, "Multi-Fidelity Design Optimisation of a Solenoid-Driven Linear Compressor," Actuators, **9**(2), p. 38.

Downloaded from asmedigitalcollection.asme.org/appliedmechanics/article-pdf/89/4/041002/6817042/jam_89_4_041002.pdf by University Catholique De Louvain-Uclouvain user on 04 November 2026